MODERN HIGH PERFORMANCE ANGLE MEASURING SYSTEMS BASED ON MONOLITHIC OPTICS

EDWARD DOWSKI, GREGORY JOHNSON, AND NELSON CLAYTOR

Ascentia Imaging, Inc, 3133 Indian Road, Boulder, CO 80303

Abstract: We describe modern angle measuring systems based on monolithic optics and modern information theory. These systems have a large field of view, no moving parts, small size, low weight and the lowest possible costs in high volume applications. In addition, the accuracy and precision of these angle measuring systems can be on the order of arc seconds or micro radians. We describe these systems as well as application to six degree of freedom localization and angular velocity estimation.

1. Introduction

Accurate and precise measurement of angles is fundamental in a large number commercial, industrial and military applications that require estimation of the locations of application-specific objects in up to six degrees of freedom (6 DOF). An angle measurement sensor ideally suited to these applications should have a wide field of view (FOV), the ability to simultaneously measure multiple angles, have the potential for high speed, have no moving parts, small size, low weight and low power, and in applications that have large production volumes, the lowest possible costs.

There are a large number of classical angle measurement sensors that significantly differ from our monolithic sensors. The use of imaging cameras are one of the most common means of measuring angles [1,2,3]. Camera systems have many applications, especially since the wide availability of low-cost camera modules. The accuracy, precision and speed of these systems is fundamentally limited by the number of pixels on the sensor. Greatly increasing the number of pixels in order to increase the measurement accuracy and precision negatively influences the potential system cost and speed.

Interferometers can be used as extremely precise wavelength-scale angle measuring devices [4, 5]. These types of systems necessarily have a very narrow field of view, compared to imaging systems. Another narrow field of view angle measurement system is an autocollimator [6], which often used in the alignment of optical elements, for example. Some configurations of autocollimators can also be used to measure rotation angles [7].

Another common type of system used to measure angles are laser trackers or total stations [8,9,10]. These systems typically use a narrow FOV coherent ranging system, such as an absolute distance measurement [11] system, and a pair of calibrated rotation stages to rotate the system over a very wide FOV. These systems can be very accurate and precise over a large FOV but can also typically track only a single point at a time. The use of rotation stages means that the size and weight of these systems is also relatively high.

One last system for measuring angles is called iGPS. These systems use a series of rotating near infrared (NIR) lasers at fixed positions around some measurement volume, each with a

unique rotation rate. A set of receivers mounted at a known separation is used to take a multitude of measurements within the volume. An algorithm is then used to deduce, or bundle, the Tx's thereby estimating their position in 3D [12]. The iGPS system is very powerful but also physically very large due to the series of rotating lasers.

The ability to fabricate and assemble specialized arrays of optical elements with optical precision, and knowledge of information theory related to the detection and estimation of information about distant sources both led to the development of our monolithic sensors. The combination of specialized optical modules and information theory can lead to miniature, accurate and precise measurement systems that have no moving parts and a wide FOV. A somewhat analogous system to our system is the well-known phased-array radar [13]. Both systems can be designed and tested via concepts of information theory such as Fisher Information and the Cramer-Rao bound [14,15]. Collectively, this results in multi-channel optical systems that are pure information gathering devices that achieve the angle measurement performance of instruments with the physical robustness of the cell phone camera in your pocket.

An example of a monolithic optic multi-channel angle sensor is shown in Figure 1. This sensor is composed of two 4x4 arrays of specialized injection-molded aspheric optics, an aperture array, two spacer arrays and a specialized mask array. The planar arrays are assembled and bonded through mechanical reference features and form a mechanically stable monolithic module. The FOV of the optical module is about 40 x 40 degrees with a weight of about 10 grams and a volume under 5 cm^3. Light from each optical channel is captured by single-pixel silicon detectors following the mask array. The detectors are preferably relatively large to minimize spatial alignment requirements. Collectively the optical module and detector board form the analog uniqueness of this angle measurement sensor, enabling a wide FOV, high precision and very low intrinsic cost in volume applications. The single pixel detectors enable high-speed sampling with relatively low power as there are only 16 pixels.

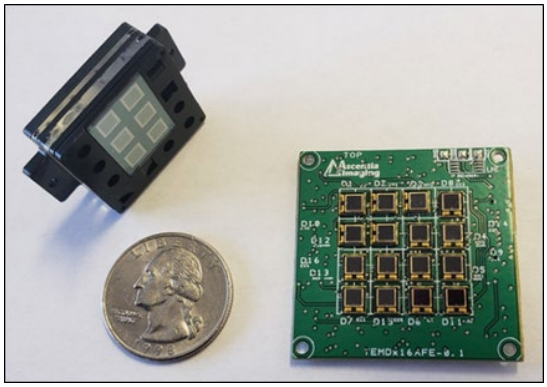

Figure 1: Monolithic optical module and single-pixel detector board.

In operation, near infrared (NIR) light from distant temporally modulated sources is captured by the 16 unique optical/digital channels. This light can be projected from distant LEDs and/or laser diodes or reflected off distant objects. The configuration of the light sources is typically application specific. For example, three or more uniquely modulated LEDs can be mounted to an object to be tracked relative to a fixed point. Or three or more LEDs can be

mounted in fixed positions throughout a volume in order to track objects that contain the optical module and detector board moving through the volume.

As the single-pixel detectors capture no spatial information, temporal modulation/demodulation is used to identify different light sources. Temporal modulation also enables reliable operation when the sun in within the FOV of the system. With the addition of the mask plane, most channels are unique and produce orthogonal signals as a function of angle to a light source. This orthogonality of the signals enables fast and precise estimation of the angles to the distant sources. The update rate, angle precision and range to the distant sources are all part of a system-wide trade-space.

Below we describe more about the system layout in Section 2, an application example of 6 DOF localization estimation in Section 3, and in Section 4 we describe using the specialized nature of the optical module to directly measure 2D angular velocity as well as angle.

2. Optical/Digital System Layout and Overview

A conceptual view of the overall optical/digital system of these sensors is given in Figure 2. From left to right, the different planes on Figure 2 represent the color filter (CF), lens plane #1 (L1), spacer #1 (S1), lens plane #2 (L2), spacer plane #2 (S2) and the mask plane (Ma). The detectors and transimpedance amplifier circuitry are denoted by D/TIA, the analog-to-digital converters are shown as A/D and the signal processing to estimate angle from the digital signals is described as DSP. Prior to the mask plane, each optical channel is essentially identical.

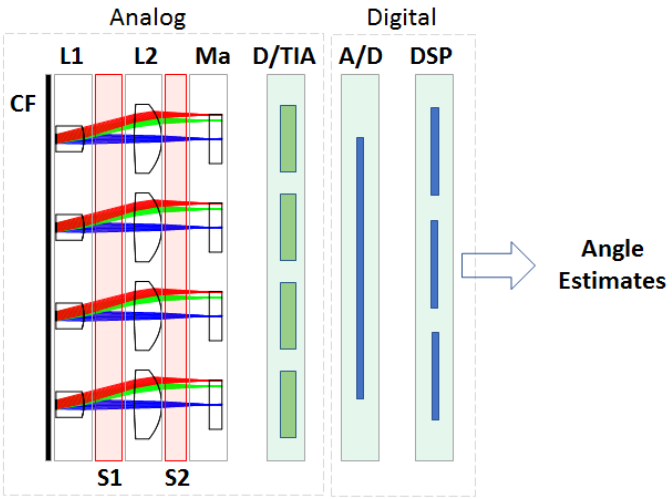

Figure 2: Multi-channel optical/digital layout

The color filter is a custom formulation of a light absorbing dye that acts to remove optical wavelengths below about 950 nm. The detectors do not absorb light past about 1000nm. The collection then has an optical band-pass of about 50 nm.

The lens arrays and spacers are designed to form an essentially telecentric optical system, where light strikes normal to the mask plane. The analog processing section contains a high-gain transimpedance amplifier (TIA) that converts current from the detectors to voltages suitable for sampling by the A/D. The A/D samples all channels simultaneously.

The mask plane contains a number of unique features. Six of the channels contain one dimensional lithographic on/off bars, four of the channels contain one dimensional linearly absorbing structures, and the remaining six channels, situated around the perimeter of the optical module are clear (i.e. no mask) in order to enable a spatially accurate representation of the mean wave front intensity.

These systems are designed via information theory. A fundamental result of information gathering with multiple channels observing the same parameters is that signals from different channels should ideally be orthogonal to signals from other channels. In this case, the mask plane acts to produce signals as a function of angle that are orthogonal to signals from the other channels. The primary means of producing orthogonal channels is to design the masks such that sets of optical channels have a sine and cosine intensity response with angle. The combination of lithographic bars and specially designed optics produce signals whose intensity closely approximates quadrature sinusoids with angle. It is well known that these types of signals are orthogonal.

.

The portion of the mask plane that contain the lithographic bars is shown conceptually in Figure 3. The width of the actual bars is much smaller than that shown, on the order of 25 micrometers. The top sets of lithographic bars, labeled Vs and Vc, are related to forming high precision vertical angles. The sets of lithographic bars labeled Hs and Hc are related to forming high precision horizontal angles. The optical elements/spacers prior to the lithographic bars have been designed so that the pass band of the optical MTF includes only the fundamental spatial frequency of the lithographic bars. The spatial harmonics of the square wave bars are not passed by the MTF. The result is essentially a sinusoidal signal that is a function of the angle to a source.

In order to avoid parallax, or range-dependent angular changes, the primary channels that measure vertical angles are positioning along a horizontal line, while the primary channels that measure horizontal angles lie along a vertical line. The two sets of lithographic bars labelled Vp and Hp purposely enable parallax information related to vertical and horizontal angles respectively. The effect of these parallax lithographic channels is to allow some range estimation for sources based on parallax.

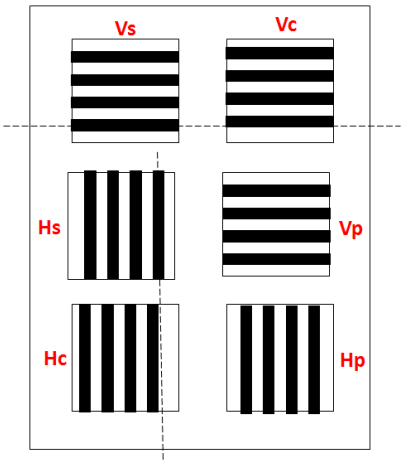

Figure 3: Layout of the lithographic bars.

Notice that the bars of the vertical channels Vs and Vc are purposely vertically shifted relative to one another by ½ bar width, which is ¼ of a period of a bar/space or 90 degrees, relative to their respective optical axes. The horizontal channels Hs and Hc are horizontally shifted by the same 90 degrees. As seen in Figure 2, light from angles from distant sources is directed to different spatial regions of the mask plane. The spatial offsets of the sets of lithographic bars then translate to signals with intensity that closely approximate sine and cosine or orthogonal quadrature channels of the system as a function of angle.

The channels that contain the linearly absorbing material have a one-dimensional ramp-like physical form. The material is a custom formulation moldable optical plastic that has high absorbance at about 950nm. These channels produce signals where the intensity is approximately a linear function of the angle to a source.

Figure 4 shows a graphical representation of the actual intensity output vs angle of three channels that are designed to measure light in one of two orthogonal directions (such as vertical or horizontal). The combination of the two sinusoidal channels that are separated by 90 degrees in phase approximate a circular form in intensity as a function of angle. With the addition of a one dimensional linearly intensity varying channel, the three-signal set form a one-parameter representation of the angle to a source, as seen in Figure 4. As the output from these optical/digital channels prior to the A/D is purely analog these one-parameter curves representing angle are completely continuous. Any particular angle to a distant source is then represented somewhere along this one-parameter curve. Calibration of the systems enable labeling the curves as a function of angle. Signal processing of the resulting sampled signals estimates angles based on these calibration curves.

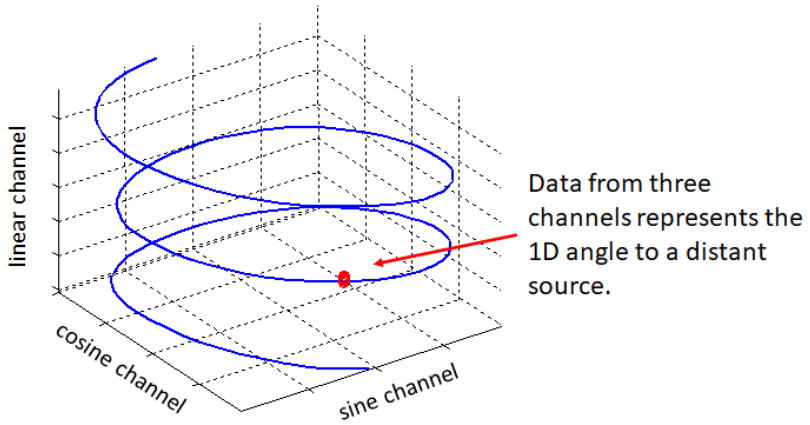

Figure 4: Actual data from three channels (one sine channel, one cosine channel and a linear channel) as a function of angle form a one parameter curve. Location along the curve determines the actual angle to a distant source.

Actual data in this 3-dimensional one-parameter space, such as the red region in Figure 4, will lie somewhere along the set of curves that define the optical module and analog electronics. The signal-to-noise ratio (SNR) of the analog signals determine the variation of the actual data about these one-parameter curves, or potential information contained in the data of the actual angles. Signals with a higher SNR will have a smaller statistical variation along these curves (i.e. high angle information), signals with a lower SNR will have a larger statistical variation along the curves (i.e. lower angle information).

Due to the analog nature of the system, the angular precision is then linearly related to the SNR of the signals. As the underlying signals are analog (i.e. not quantized) the upper limit of precision is completely determined by photon shot noise, analog circuitry noise, and the number of bits in the digitally sampled signals when using digital processing. Accuracy of the system as a function of angle is determined by the quality and accuracy of the calibration that describes the multi-channels signals vs angle.

This angular precision vs SNR then leads to a broad system-level trade-space. The SNR of digitally sampled signals is determined by the light density reaching the apertures of the optics, photon shot noise, analog electronic noise, the A/D sampling speed (and bandwidth) and the optical/digital sensitivity of the system. For example, doubling the amount of light reaching the sensor (by increasing the current of a modulated LED for example) will essentially double the SNR of the sampled signals, which will increase the angular precision by about a factor of two. Increasing the sampling rate of the A/D say by a factor of two will then decrease the number of sampled electrons by about a factor of two, leading to a reduction of SNR and precision by about the same factor of two. Increasing detector sensitivity, say by use of avalanche photodiodes, can directly increase angular precision by the SNR gain of the detectors, which can often achieve 10X-100X for a constant number of photons. Overall, only nano-watts of optical power measured at the apertures is needed to yield approximately arc seconds or micro radian angular precision.

3. 6DOF Localization Example

An example of 6 DOF localization is described with Figure 5. In this example, there are three sinusoidally temporally-modulated LEDs (or Tx's) with estimated relative locations in three dimensions, shown at the left. On the right are the estimates of seven previously unknown positions and orientations of an optical sensor module (or Rx). In this example the precision of the measured angles was about 4 arc seconds (~ 20 micro radians).

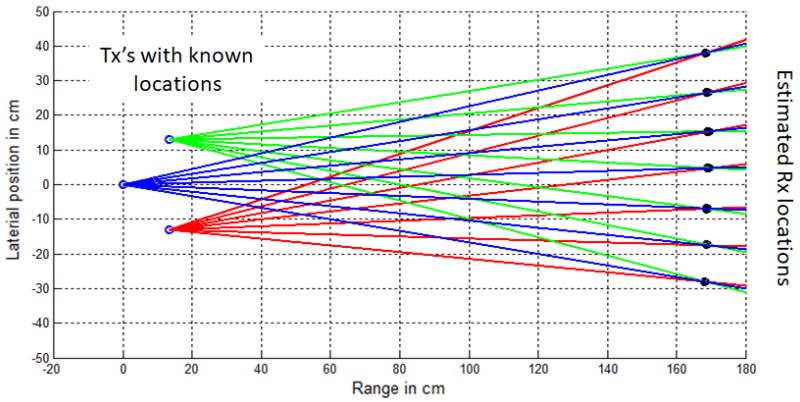

Figure 5: Layout of 3 Tx's to estimate 6DOF locations of an Rx.

In practice, the relative 3D locations of a collection of LEDs can be measured or estimated in many ways. One practical way to estimate the location of the LEDs is through a measurement process where one or more parameters of either the Tx set or Rx positioning is assumed known. For example, the relative locations of two or more LEDs in one dimension can be carefully measured. Or, a one-dimensional distance between Rx positions can be assumed known. A constrained optimization with the resulting Rx angle data can then be used in order to estimate the locations of both the Tx's and Rx's. The assumed known information constrains the

solution to the proper scale. The accuracy of the estimated Tx positions is mainly limited by the accuracy of the Rx angles as well as the number and range of angles used in the optimization. After the relative Tx locations have been estimated, general Rx locations can be directly estimated.

The output from the Rx for the example in Figure 5 represents the three angles to the three modulated LED's, or Tx's. Conceptually tracing rays from the Tx locations, with the measured angles from the Rx, then leads to the intersection of the rays or the estimated location of the Rx. Ideally, a set of rays from the Tx's will all intersect at some distant point. Finding a least-squares solution to the ray intersection over roll, pitch and yaw parameters then leads to an estimate of Rx locations and ray intersection error. This ray error can be used as an accuracy metric for the overall system. For the data of Figure 5 the mean error in the ray intersections is about 1/4th of a micrometer, which strongly suggests a highly accurate system.

In this type of configuration, the physics of stereo triangulation limit the estimated localization precision of the Rx. The range dimension is often the least precise localization parameter when the system configuration has a stereo form. From information theory we can show that the mathematical information of range can be described by Fisher Information [13]. The inverse of the Fisher information, or the Cramer-Rao bound [13,14], can then describe the expected ideal variation of estimates of range or range precision. A simplified mathematical form for the overall system can then lead to a Fisher Information of range given by:

$$\mathrm{I} = SNR \ \frac{Range}{B^2} \tag{1}$$

where SNR is the system signal-to-noise ratio, and B is the baseline between the two most-separated LEDs. The expected ideal variation of estimates of range, or Cramer-Rao bound, can then be given by

$$\mathrm{J} = \frac{B^2}{SNR * Range} \tag{2}$$

The baseline B of the Tx's in Figure 5 is about 26 cm, with a range of about 170cm. The measured standard deviation of the estimated range is about 0.25mm. This translates to an effective system SNR of about 160. Changes in either range to the Tx's or the baseline of the Tx's will then lead to expected changes in the range precision given by equation 2.

Figure 6 displays the estimated Rx positions in more detail. For simplicity spatial motion was only in two dimensions. The left graph of Figure 6 shows twenty measurements made for each of the seven Rx positions. The right graphs show two individual sets of measurements in more detail. The top right graph shows the variation for the measurements near the lateral position of 40 cm, the bottom right shows the variation of the measurements for the lateral position near the lateral position of about 5 cm. As in most triangulation systems, the error profile is angled towards the direction of the centroid of the set of Tx's. The standard deviations of range for this example, is about 0.25 mm. The standard deviation of the other two spatial dimensions is about 20 micrometers, or about 10X more precise than the range estimates.

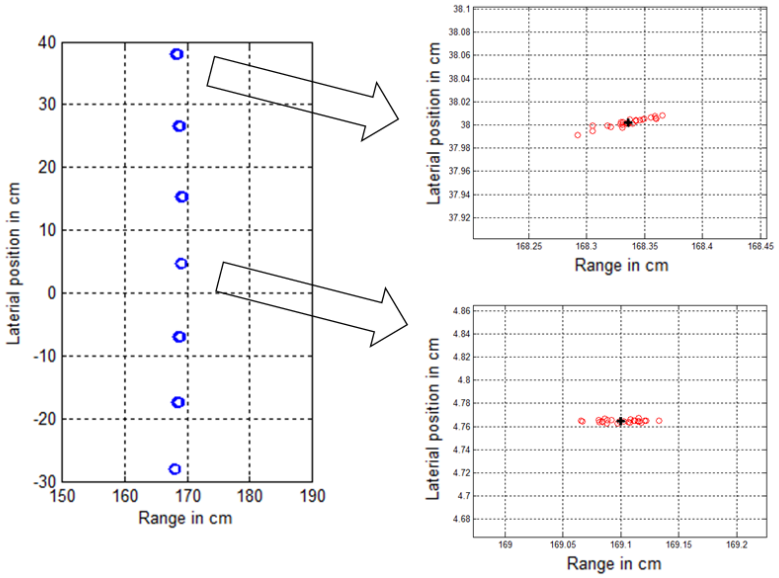

Figure 6: Estimated spatial positions and expanded views.

The wide difference in localization precision between range and spatial coordinates orthogonal to range highlight some important aspects of these systems. When a set of Tx's and Rx's are used on their own to estimate spatial localization or 6 DOF localization, the baseline between the known points must be large enough to ensure adequate range precision, given the other relevant system parameters. In some systems the baseline can be increased beyond the 40 x 40 degree FOV of a single Rx. Grouping multiple optical modules in order to span a much larger system FOV can lead to a measurement sensor with basically any FOV.

If these systems are used with a specialized range measuring device, such as a laser range-finder (or possibly a laser tracker or total station) the precision of all three spatial coordinates can be estimated to a high precision with the entire system having no moving parts and a smaller baseline than otherwise. Having no moving parts, besides having significant, size and weight advantages, also enables the estimation of very small changes in angle as there is no friction or hysteresis to overcome, as is common with mechanical motion.

Estimation of the three rotation angles in 6 DOF measurements (roll, pitch and yaw) are difficult with classical systems, often because only a single point can be measured at any one time. But, with our modern angle estimation systems these angles are directly produced. Figure 7 shows the mean rotation angles for the data of Figure 5. The yaw angles were purposely varied for the different Rx positions of Figure 5, with the estimated angles shown in Figure 7. Non-square motion/rotation of the Rx, relative to the calibration data, leads to the results in the low-slope variation of the roll and pitch angles.

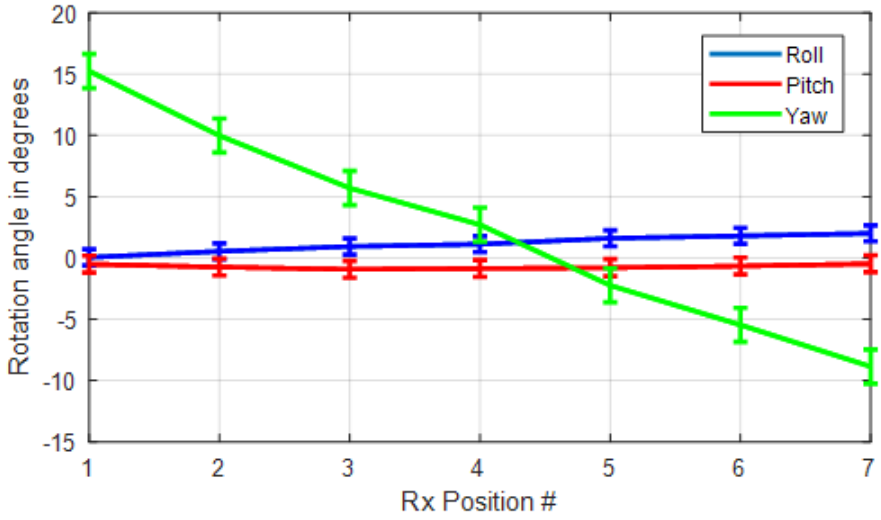

Figure 7: Estimated Roll, Pitch and Yaw for each Rx positions.

The measured statistical precision of the roll, pitch and yaw angles from Figure 7 are shown via error bars. The units for the statistical precision is arc seconds (not degrees). For example, the measured statistical precision of the yaw angles is about +/- 1.5 arc seconds. The measured statistical precision of roll is less than +/- 1 arc second. The precision of these angles is on the order of magnitude of the fundamental angular precision of the angle sensor, which can often be low arc seconds (low tens of micro radians).

4. Localization with Motion Example

These monolithic angle measurement sensors have been designed to provide maximum angle measurement sensitivity and precision. The specialized nature of the systems, particularly the orthogonal quadrature channels, also enables direct measurement of angular motion, in addition to the measurement of angles. As seen from Figures 2 and 3, angles to a source are converted to spatial position on the lithographic bars by the telecentric optics. Angular temporal motion will then be converted into temporal signals through the same manner, and in effect, will temporally modulate the signals from the orthogonal quadrature channels enabling direct measurement of angle vs time or angular velocity and/or acceleration.

As the signals from the sources are temporally modulated, the raw signals from the analog Rx module are also temporally modulated. The intensity of the particular signal is a function of the angle to the source. For example, the non-negative signal from one of the quadrature channels can be approximated as:

$$\text{Signal}(t,\text{angle}) = (\sin(w_{angle} * \text{angle}) + K) * (\sin(w_{mod}\, t) + M) \qquad (3)$$

where w_{angle} is approximately 2π (or the period is approximately one degree) and w_{mod} is $(2\pi f)$ where f is the temporal modulation frequency. The terms K and M are non-negative bias values.

The magnification of the optics and the spatial period of the lithographic bars dictate that one period of the lithographic bars occupy one degree of angular deviation of the source. For the following, assume a temporal modulation frequency of f =1000 Hz.

Figure 8 describes a simulated example of the raw output from a signal related to the lithographic bars with and without angular motion of the source. With no relative angular motion between the source and the Rx, the raw signal is a constant-amplitude sinusoid with the amplitude being related to the angle to the source. With constant angular motion, the amplitude of the temporal sinusoid changes with time dependent on the velocity and acceleration of the source or the relative angular rotation between the source and the Rx. The signal that represents the angular motion in Figure 8 has then both temporal modulation and a time-varying amplitude due to source angular motion. The velocity of the angular motion for this example is 50 degrees per second (dps).

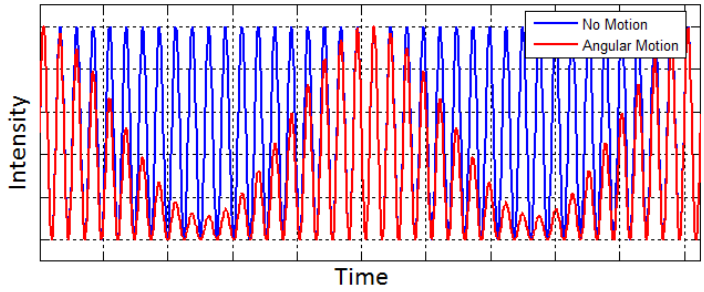

Figure 8: Raw temporal signal from a channel with the lithographic bars with and without angular motion of the source.

This time-varying amplitude related to the source angular motion can also be considered as a change in the temporal modulation of the fundamental source temporal modulation. Figure 9 shows the temporal frequency spectrum of the data in Figure 8. The no-motion signal, or the constant-amplitude 1000 Hz sinusoid has a pronounced peak in the temporal frequency spectrum at 1000 Hz. The signal with 50 dps of angular motion, in contrast, has temporal frequency peaks at 1000 Hz and 1000 +/- 50 Hz. The angular motion in effect temporally modulates the 1000 Hz signal generating sidebands spaced about the central peak. Detection and estimation of these sidebands around the known sinusoidal source modulation frequency for all the lithographic bar channels then enables direct estimation of angular velocity and acceleration.

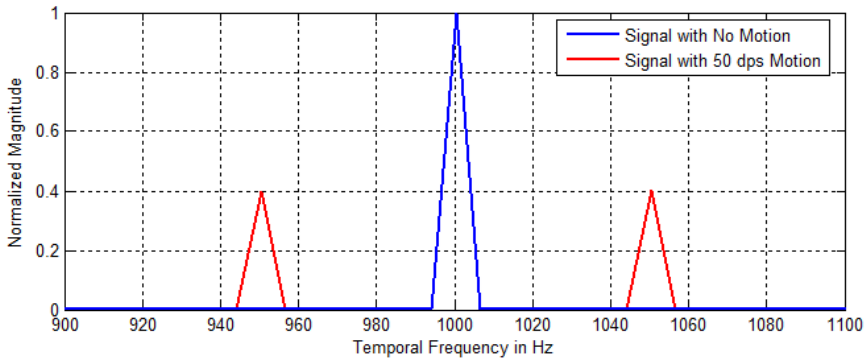

Figure 9: Temporal frequency spectrum of the signals of Figure 8.

Experimental data related to the temporal frequency spectrum vs time (or short-time Fourier Transform) for a source with both angular velocity and acceleration is shown in Figure 10. For this example, the temporal modulation of the source was again 1000 Hz. The source motion consisted of an angular acceleration to a constant 15 dps, and then a deceleration to no angular motion. Notice that the temporal spectrum contains just the main peak at 1000 Hz initially. The sidebands appearing on either side of 1000 Hz show angular acceleration to a constant angular velocity and then an angular deceleration. The temporal frequency of the sidelobes during the constant-velocity region is 1000 +/- 15 Hz. Because of the particular 1 degree / period of the lithographic bars, these 15 Hz sidelobes then translate to 15 dps angular velocity. Depending on the sampling rate of the A/D and the period of the lithographic bars, the sensitivity and precision of the angular velocity and acceleration estimation can be customized for a particular expected range of motion.

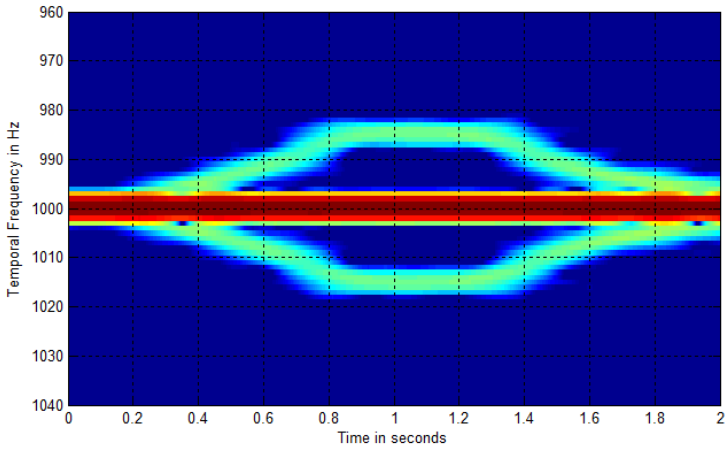

Figure 10. A short-time Fourier transform of raw data related to a temporally modulated source with angular acceleration, constant motion and deceleration.

5. Conclusions

Modern monolithic angular measurement systems can be considered as pure information gathering systems, physically similar to the cell phone camera in your pocket. Both systems share small size, low weight and high mechanical robustness. Angular measurement systems in contrast, have multiple channels gathering unique orthogonal information related to the angles to distant sources. These orthogonal channels enable very fast, accurate and precision measurement of angles to distant sources, source velocity and acceleration.

These angular measurement systems are intended to be sub-systems in larger measurement and/or control systems. The very general nature of these systems leads to a very general application-specific trade-space involving system variables such as electronics speed and cost, electrical power and overall system Rx/Tx configuration. The application-specific nature of this trade-space can sometimes lead to systems involving companion devices such as laser range-finders for relatively inexpensive measurements of complimentary system information, such as range. The combination can then measure 6 DOF localization with the accuracy and precision being similar for every dimension.

Disclosures. The authors declare no conflicts of interest.

Data availability. Data underlying the results presented in this paper are not publicly available at this time but may be obtained from the authors upon reasonable request.

References

1. E. M. Mikhail, J. S. Bethel, J. C. McGlone, Introduction to Modern Photogrammetry, Wiley, New York, 2001
2. Yihong Wu, Fulin Tang, Heping Li, Image-based camera localization: an overview. Visual Computing for Industry, Biomedicine and Art 1, Article number 8 (2018).
3. M. Lu, C. Hsu and Y. Lu, "Distance and angle measurement of distant objects on an oblique plane based on pixel variation of CCD image," *2010 IEEE Instrumentation & Measurement Technology Conference Proceedings*, 2010, pp. 318-322.
4. Masroor Ikram, Ghazanfar Hussain, Michelson Interferometer for Precision Angle Measurement, Applied Optics, Feb 1999, 38(1):113-120.
5. J. Tkaczyk, G. Budzyn and J Rzepka, Absolute interferometric angle measurement, J. Phys.: Conf. Ser. 1149 012030, 2018.
6. Yan Guo, Haobo Cheng, Yongfu Wen, and Yunpeng Feng, Three-degree-of-freedom autocollimator based combined target reflector. Applied Optics, Vol. 59, Issue 8, pp. 2262-2269, (2020)
7. Yusuke Saito, Yashikazu Arai, Wei Gao, Detection of three-axis angles by an optical sensor, Sensors and Actuators A: Physical, Vol 150, Issue 2, 25 March 2009, pg 175-183.
8. Walker J., Awange J.L. (2018) Total Station: Measurements and Computations. In: Surveying for Civil and Mine Engineers. Springer.
9. Bala Muralikrishnan, Steve Philips, Daniel Sawyer, Laser Trackers for large-scale dimensional metrology: A review. Precision Engineering, Volume 44, April 2016, pages 13-28
10. Chang'an Hu, Shutong Luo, Wanze Lij, Dongyan Cai, Application of laser tracker in the industrial measurement field. Journal of Physics Conference Series, Vol. 1820(2021)012119, March 2021.
11. René Dändliker, Absolute distance measurements. Proc. SPIE 2778, 17th Congress of the International Commission for Optics: Optics for Science and New Technology, 2778EJ (1 September 1996)

12. C. Depenthal, "Path tracking with IGPS," *2010 International Conference on Indoor Positioning and Indoor Navigation*, 2010, pp. 1-6

13. A.W. Rihaczek, *Principles of High Resolution Radar,* McGraw-Hill, New York, 1969.

14. L. L. Scharf, *Statistical Signal Processing* 1Addison-Wesley, Reading MA, 1991.

15. L. L. Scharf and L. T. McWhorter, "Geometry of the Cramer-Rao bound," *[1992] IEEE Sixth SP Workshop on Statistical Signal and Array Processing*, 1992, pp. 5-8